Draft version November 8, 2017
Preprint typeset using LaTeX style AASTeX6 v. 1.0

SHORT-LIVED CIRCUMSTELLAR INTERACTION IN THE LOW-LUMINOSITY TYPE IIP SN 2016bkv

Griffin Hosseinzadeh[1,2], Stefano Valenti[3], Curtis McCully[1,2], D. Andrew Howell[1,2], Iair Arcavi[1,2,9], David Guevel[1,2,4], Leonardo Tartaglia[3,5], Liming Rui (芮黎明)[6], Xiaofeng Wang (王晓锋)[6], Fang Huang (黄芳)[6], Hao Song[6], Tianmeng Zhang[7], and Koichi Itagaki (板垣公一)[8]

[1] Las Cumbres Observatory, 6740 Cortona Drive, Suite 102, Goleta, CA 93117-5575, USA; griffin@lco.global
[2] Department of Physics, University of California, Santa Barbara, CA 93106-9530, USA
[3] Department of Physics, University of California, 1 Shields Avenue, Davis, CA 95616-5270, USA
[4] Harvard-Smithsonian Center for Astrophysics, 60 Garden Street, Cambridge, MA 02138, USA
[5] Department of Astronomy/Steward Observatory, 933 North Cherry Avenue, Tucson, AZ 85721-0065, USA
[6] Physics Department and Tsinghua Center for Astrophysics, Tsinghua University, Beijing, 100084, China
[7] National Astronomical Observatory of China, Chinese Academy of Sciences, Beijing, 100012, China
[8] Itagaki Astronomical Observatory, Yamagata 990-2492, Japan

ABSTRACT

While interaction with circumstellar material is known to play an important role in Type IIn supernovae (SNe), analyses of the more common SNe IIP and IIL have not traditionally included interaction as a significant power source. However, recent campaigns to observe SNe within days of explosion have revealed narrow emission lines of high-ionization species in the earliest spectra of luminous SNe II of all subclasses. These "flash ionization" features indicate the presence of a confined shell of material around the progenitor star. Here we present the first low-luminosity SN to show flash ionization features, SN 2016bkv. This SN peaked at $M_V = 16.1$ mag and has expansion velocities around maximum light of $\lesssim 1500$ km s^{-1}, placing it at the faint/slow end of the distribution of SNe IIP (similar to SN 2005cs). The light curve of SN 2016bkv is also extreme among SNe IIP: it has a very strong initial peak and a very small fall from the plateau to the nickel tail. We investigate the nature of the progenitor of SN 2016bkv by analyzing the properties of its light curve and nebular spectra. Our results demonstrate that circumstellar interaction plays a role even in low-luminosity SNe IIP. Conversely, they imply that the range of luminosities of SNe II is not solely driven by the presence of circumstellar material.

Keywords: supernovae: general — supernovae: individual (SN 2016bkv)

1. INTRODUCTION

The majority of massive ($M_{\rm ZAMS} \gtrsim 8$ M$_\odot$) stars end their lives as Type II supernovae (SNe), i.e., those with hydrogen-rich spectra (see Smartt 2009, for a review). Broadly speaking, SNe II can be divided into two subclasses. SNe IIP/L have light curves that plateau (P) or decline linearly (L) for roughly 100 days before falling to a radioactive-decay-powered tail (Barbon et al. 1979). SNe IIn have spectra domniated by narrow (n) hydrogen emission lines, indicating strong interaction with circumstellar material (CSM; Schlegel 1990; Chugai 1991). Hereinafter we will use "SNe II" to refer to SNe IIP and IIL as a single class, excluding SNe IIn.

SNe II peak in the range $-14 \gtrsim M_B \gtrsim -18$ mag (Patat et al. 1994) and show a tight correlation between luminosity and photospheric expansion velocities (Hamuy & Pinto 2002; Pejcha & Prieto 2015). At the faint/slow end of this distribution is a group of events referred to as low-luminosity (LL) SNe II (Pastorello et al. 2004; Spiro et al. 2014), exemplified by the nearby, well-studied SN 2005cs, whose red supergiant (RSG) progenitor star was detected by Maund et al. (2005) and Li et al. (2006) in pre-explosion images taken by the *Hubble Space Telescope* (*HST*). Several models have been proposed to explain LL SNe II, including high-mass RSGs exploding as fallback SNe (Turatto et al. 1998; Zampieri et al. 1998) and low-mass RSGs exploding as electron-capture SNe (Chugai & Utrobin 2000). Pumo et al. (2017) claim that the ratio of the explosion energy to the ejected mass controls the plateau luminosity of SNe II, where smaller ratios are less luminous (see their Figure 5).

Interaction with CSM traditionally has not been considered significant in SNe II, since broad P Cygni lines dominate their spectra. However, recent efforts to obtain spectra of SNe within days of explosion have resulted in the discovery of narrow emission features in a significant fraction of early spectra of SNe II (18% of those observed within 5 days of explosion; Khazov et al. 2016). Early

[9] Einstein Fellow

examples of these features include SNe 1983K (Niemela et al. 1985), 1993J (Benetti et al. 1994; Garnavich & Ann 1994; Matheson et al. 2000), 1998S (Leonard et al. 2000; Shivvers et al. 2015), and 2006bp (Quimby et al. 2007). Gal-Yam et al. (2014) first coined the term "flash spectroscopy" to describe this emission, produced as the CSM recombines after being ionized by the initial shock breakout flash. More recently, Yaron et al. (2017) observed flash spectra of the Type II SN 2013fs changing on hour time scales.

Intriguingly, Khazov et al. (2016) suggest that the presence of flash ionization features may be correlated with luminosity; in fact, all their flash ionization spectra are from events with peak absolute magnitudes $M_R < -17.5$ mag. This implies that more luminous events maintain higher temperatures at early times, enabling high-ionization lines to persist in their spectra long enough to be detected.

The object presented here, SN 2016bkv, is a SN II discovered soon after explosion. With a peak absolute magnitude of $M_V = -16.1$ mag and Hα expansion velocities under 1500 km s^{-1}, it greatly resembles SN 2005cs and other LL events in the literature. However, unlike any previous LL SN II, its pre-maximum spectra are dominated by narrow emission lines from high-ionization species, making it the least luminous SN for which flash ionization of the CSM has been detected. Below we report observations of SN 2016bkv and discuss its implications for the role of CSM interaction in SNe II.

2. DISCOVERY

Itagaki (2016) discovered SN 2016bkv on 2016 March 21.70 UT at 17.5 mag using an unfiltered Celestron 14 inch (35 cm) telescope. Based on the nondetection of Ross et al. (2016) on March 19.29 at an unfiltered limiting magnitude of 17 mag, we conclude that the SN was discovered within a few days of explosion; specifically we adopt March 20.5 (MJD$_0 = 57467.5 \pm 1.2$) as the explosion epoch. Hosseinzadeh et al. (2016) obtained the first spectrum on March 23.5, classifying the transient as a young SN II.

At right ascension $10^{\rm h}18^{\rm m}19\overset{\rm s}{.}31$ and declination $+41°25'39\overset{''}{.}3$ (J2000), SN 2016bkv lies $30\overset{''}{.}3$ (2.11 kpc projected) from the center of the spiral galaxy NGC 3184, which has a redshift of $z = 0.001975 \pm 0.000003$ (Strauss et al. 1992) and a Cepheid-based distance modulus of $\mu = 30.79 \pm 0.05$ mag (Ferrarese et al. 1999)[10], corresponding to a luminosity distance of $d_L = 14.4 \pm 0.3$ Mpc. In the past century, NGC 3184 has hosted at least four other SNe—1921B, 1921C, 1937F (Shapley 1939)[11], and 1999gi (Type II; Schlegel 2001; Smartt et al. 2001)—and one SN impostor—SN 2010dn, which Smith et al. (2011) claim was the outburst of a luminous blue variable star.

As noted by Milisavljevic et al. (2016), images of NGC 3184 from *HST* show a star cluster at the position of SN 2016bkv. When the SN fades, it may be possible to determine the luminosity and colors of the progenitor star based on the change in flux from the cluster.

3. OBSERVATIONS AND DATA REDUCTION

In addition to unfiltered photometry from the 35 and 60 cm telescopes at Itagaki Astronomical Observatory (Yamagata, Japan), we obtained *UBVgri* photometry of SN 2016bkv using Las Cumbres Observatory's (LCO; Brown et al. 2013) robotic 1 m and 2 m telescopes located at the McDonald (TX, USA) and Haleakalā (HI, USA) Observatories, respectively, and *UBVRI* photometry using the 0.8 m Tsinghua University–National Astronomical Observatory of China Telescope (TNT; Huang et al. 2012) located at Xinglong Observatory (Hebei Province, China). Unfortunately, the *Swift* satellite could not observe the SN in ultraviolet due to a nearby bright star.

We obtained 17 optical spectra of SN 2016bkv during the photospheric phase using the robotic FLOYDS instrument, mounted on LCO's 2 m telescope on Haleakalā, and the Beijing Faint Object Spectrograph and Camera (BFOSC) and the Optomechanics Research Inc. (OMR) low-resolution spectrograph, both mounted on the 2.16 m telescope at Xinglong (Fan et al. 2016). These spectra are plotted in Figure 2. Three additional spectra were obtained during the nebular phase using the Kast Double Spectrograph (Miller & Stone 1994) on the C. Donald Shane Telescope at Lick Observatory (CA, USA) and the Low-Resolution Imaging Spectrometer (LRIS; Oke et al. 1995; Rockosi et al. 2010) on the Keck I telescope at the W.M. Keck Observatory (HI, USA). All spectra are logged in Table 1 and available for download from the Weizmann Interactive Supernova Data Repository (Yaron & Gal-Yam 2012).

Photometry measurements were complicated by the fact that the SN occurred in a bright but unresolved H II region (number 62 in the list of Hodge & Kennicutt 1983) and about 7.7" away from an even brighter star (SDSS J101819.82+412544.3; Adelman-McCarthy et al. 2007). We obtained *BVgri* reference images with LCO approximately 600 days after explosion, when the SN was much fainter than the H II region, and subtracted them from the LCO images of the supernova using PyZOGY (Guevel & Hosseinzadeh 2017), a Python image subtraction pipeline based on the optimal algorithm of Zackay et al. (2016). This is the first published PyZOGY light curve; the code is available on the GitHub page of its

[10] Note, however, that other methods give distance moduli ranging from 29.3 mag (Pierce 1994) to 31.2 mag (Jones et al. 2009).
[11] Spectra of these SNe from E. Hubble's and F. Zwicky's programs were never obtained, but they have been photometrically classified as Types II, I, and IIP, respectively (Barbon et al. 2008).

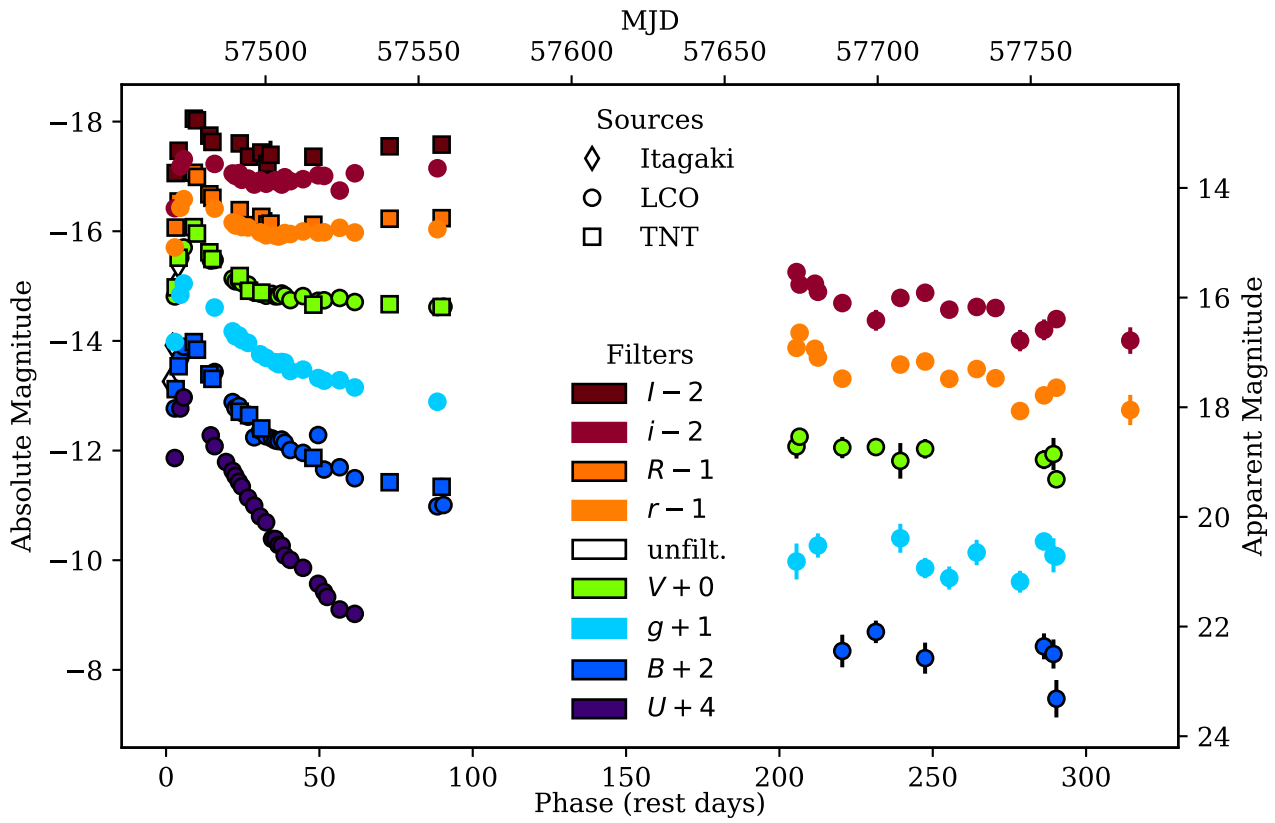

Figure 1. One year of photometry of SN 2016bkv. Late nondetections are hidden for clarity. Note the strong early bump and the small fall from plateau, which happened while the supernova was behind the sun. (The data used to create this figure are available.)

Table 1. Log of Spectroscopic Observations

MJD	Telescope	Instrument	Phase (d)
57470.5	LCO 2 m	FLOYDS	3.0
57471.0	Xinglong 2.16 m	BFOSC	3.5
57471.4	LCO 2 m	FLOYDS	3.9
57472.3	LCO 2 m	FLOYDS	4.8
57475.3	LCO 2 m	FLOYDS	7.8
57480.4	LCO 2 m	FLOYDS	12.9
57481.0	Xinglong 2.16 m	BFOSC	13.5
57487.4	LCO 2 m	FLOYDS	19.9
57491.0	Xinglong 2.16 m	BFOSC	23.5
57492.4	LCO 2 m	FLOYDS	24.9
57498.4	LCO 2 m	FLOYDS	30.8
57502.3	LCO 2 m	FLOYDS	34.7
57507.3	LCO 2 m	FLOYDS	39.7
57511.3	LCO 2 m	FLOYDS	43.7
57514.0	Xinglong 2.16 m	OMR	46.4
57526.3	LCO 2 m	FLOYDS	58.6
57550.3	LCO 2 m	FLOYDS	82.6
57724.6	Shane	Kast	256.6
57780.?	Shane	Kast	313.?
57903.3	Keck I	LRIS	434.9

lead developer, D. Guevel. We then measured aperture photometry on the difference images using `lcogtsnpipe` (Valenti et al. 2016).

We measured PSF photometry from the remaining unsubtracted images using standard PyRAF tasks (Science Software Branch at STScI 2012), with the help of `lcogtsnpipe` (Valenti et al. 2016) for the LCO *U*-band images and SNOoPY (Cappellaro 2016) for the TNT images. *UBVRI* photometry is calibrated in the Vega system to Landolt (1992) standard fields observed on the same night as the SN. *gri* photometry is calibrated in the AB system to stars in the Sloan Digital Sky Survey Data Release 8 (SDSS DR8; Aihara et al. 2011). Unfiltered photometry is calibrated to 20 nearby stars in SDSS DR6 (Adelman-McCarthy et al. 2007) by fitting blackbody spectra to their *ugriz* photometry and, for stars with reasonable fits, convolving the spectra with the spectral response curve of K. Itagaki's KAF-1001E CCD (both telescopes use the same CCD) to produce AB magnitudes. The resulting unfiltered magnitudes are not relevant to the bolometric light curve we produce in Section 4.1, but we do consider them when fitting the early light curve in Section 4.2. The photometry is plotted in Figure 1.

4. ANALYSIS

4.1. *Blackbody Fitting and Bolometric Light Curve*

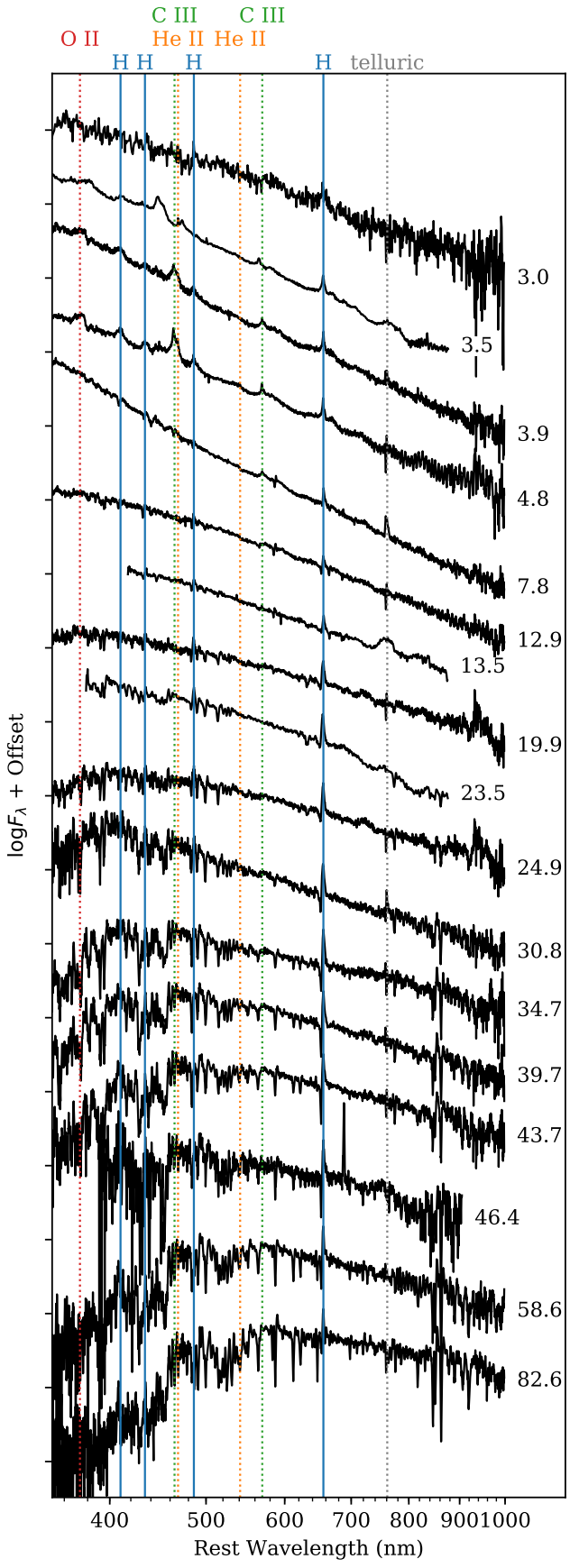

Figure 2. Photospheric spectra of SN 2016bkv with flash ionization lines marked. See Figure 7 for a more detailed line identification during the photospheric phase. Phases in days from estimated explosion are marked to the right of each spectrum. The early high-ionization lines disappear after 5 days, giving way to typical SN II spectra with very low photospheric velocities ($< 1500\,\mathrm{km\,s^{-1}}$).

We construct a bolometric light curve of SN 2016bkv by fitting each epoch of photometry with a blackbody spectrum. In order to compare to pseudo-bolometric light curves from the literature, we then integrate the blackbody spectrum only from U to I. The result is shown in Figure 3, where it is compared to bolometric light curves of other SNe II from Valenti et al. (2016).

The bolometric light curve of SN 2016bkv is extreme in two ways. First, it has a very strong peak around 7 days after explosion with respect to the plateau luminosity ($s1$ in Valenti et al. 2016). We attribute this to excess luminosity from circumstellar interaction. Second, it has a very small fall between the plateau and the radioactive nickel tail. This implies that the amount of nickel produced in the explosion is unusually large for a LL SN II. Comparing the luminosity on the tail to SN 1987A as in Hamuy (2003), we find that SN 2016bkv produced $M_{\mathrm{Ni}} = 0.01486 \pm 0.0009\,M_\odot$ of nickel. The uncertainty in this measurement is almost entirely due to the 2% uncertainty on the distance to the supernova and the 5% assumed uncertainty on the host-galaxy extinction ($A_V = 0.00 \pm 0.05$ mag).

Figure 5 shows the evolution of the blackbody temperature and radius from the fit. The temperature evolution shows an unexpected rise during six days. Because we lack photometry blueward of U, the blackbody fits are not strongly constrained at these early times, when the spectral energy distribution peaks in the ultraviolet. If this rising behavior is real, it might be related to the flash ionization of the CSM, which manifests itself in the spectra during the same time period. However, given the uncertainties in the fits, we cannot claim to have observed a significant effect.

4.2. *Shock Cooling Model Fitting*

Sapir & Waxman (2017) present a method for modeling early supernova light curves powered purely by shock cooling emission—the radiation of energy deposited in the stellar envelope by the core collapse shock wave. From the flash spectra of SN 2016bkv, we know that circumstellar interaction may contribute significantly to the early light curve, so we do not expect these models to fit well. Nonetheless, as an independent test, we wish to explore whether or not the early light curve peak can be described by a shock cooling model.

We fit our multiband light curve to the Sapir & Waxman (2017) model, with $n = 1.5$ for a RSG, using a Markov-chain Monte Carlo routine, resulting in posterior probability distributions of five parameters: the shock speed, v_{s*}; the mass of the progenitor envelope, M_{env}; the product of a numerical factor that describes the inner envelope structure, f_ρ, and the total ejected mass, M; the progenitor radius, R; and the time of explosion, t_0. For each set of these parameters, the model gives the

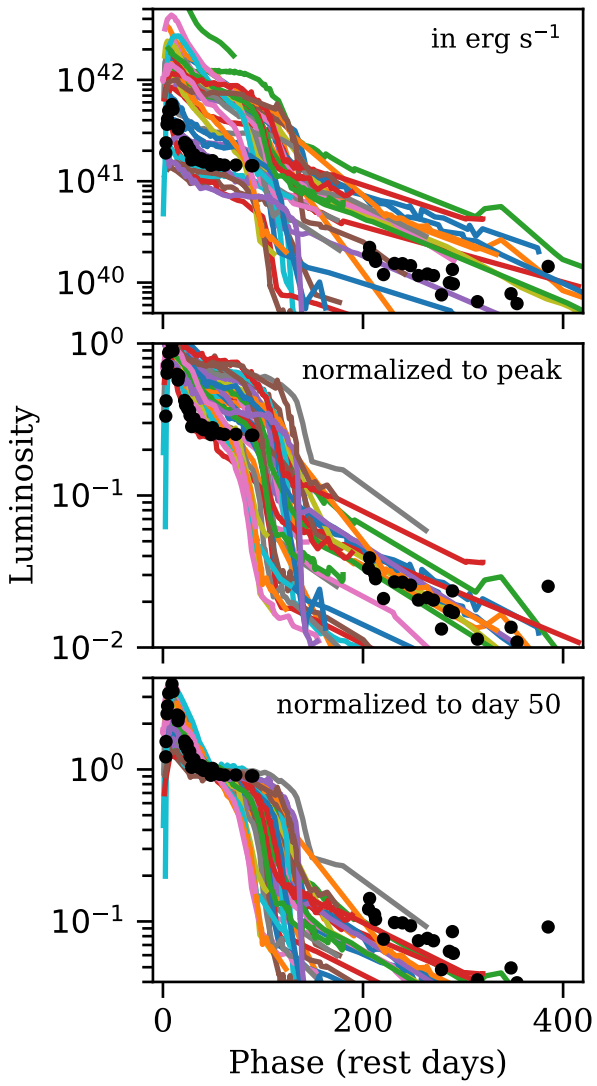

Figure 3. Bolometric light curve of SN 2016bkv (black dots) compared to the Valenti et al. (2016) sample of SNe II (colored lines). SN 2016bkv has among the most extreme initial decline slopes and the smallest fall from plateau.

blackbody temperature and radius as a function of time, which we then convert to magnitudes for each observed photometry point, simultaneously fitting all bands. Figure 4 shows the light curve fits, posterior probability distributions, and 1σ credible intervals centered on the medians.

The $M_{\rm env}$ parameter enters the models through the time-dependence of a luminosity suppression factor; to obtain light curves that decline quickly after peak, $M_{\rm env}$ must be small. However, the pre-plateau "bump" in the light curve may be caused by interaction rather than shock cooling, in which case the models would not be relevant. Indeed, Morozova et al. (2017a,b) have shown that numerical light curve models that include CSM reproduce these bumps much more faithfully than those with no CSM. Nonetheless, we continue our analysis of these shock cooling model fits for completeness.

Using Sapir & Waxman's approximation to f_ρ, we can disentangle the total ejected mass from f_ρ:

$$f_\rho M \approx \sqrt{\frac{M_{\rm env}}{M - M_{\rm env}}} M$$

This gives $M \approx 2.6\,M_\odot$ and $f_\rho \approx 0.48$. We then estimate the ratio of the explosion energy to the ejected mass using approximation of Matzner & McKee (1999), keeping in mind that the result depends on the previous approximation as well:

$$\frac{E}{M} \approx 0.907 f_\rho^{0.382} v_{\rm s*}^2 = 3.0 \times 10^{49}\,{\rm erg}\,M_\odot^{-1}$$

This is slightly higher than for the LL SNe II in the sample of Pumo et al. (2017, see Figure 6), but still lower than for their intermediate-luminosity category.

Ultimately, we conclude that shock cooling models do not fit the pre-plateau bump in early light curve of SN 2016bkv. This may be further evidence that CSM interaction contributes significant luminosity even in the week after the flash ionization features disappear from the spectra.

4.3. *Spectral Modeling*

Because of their low photospheric velocities, LL SNe IIP provide a good opportunity to identify which elements contribute to their spectra. To aid in this identification, we use SYN++ (Thomas et al. 2011) to produce a synthetic spectrum that resembles our observed spectrum from 34.7 days after explosion. We chose this spectrum because it has a high signal-to-noise ratio, and many strong P Cygni lines are visible. Figure 7 compares the synthetic and observed spectra. The synthesis parameters are listed in the SYN++ input file, which is available in the online journal.

At this phase, the blue half of the optical spectrum is dominated by iron and titanium lines. These two elements plus calcium, sodium, and hydrogen can account for nearly all of the observed features. The most notable feature of our result is that the range of velocities necessary to reproduce the observed spectrum is only 100–2000 km s^{-1}. Likewise, the photospheric velocity is 1000 km s^{-1}. Since this is near the resolution of our spectrograph, it is likely that the true ejecta velocity is lower. The photospheric temperature of our model is 7500 K, close to the blackbody temperature we calculate for this phase in Section 4.1, and the ion temperatures of 10^4 K are reasonable for the interior of the ejecta (although the synthetic spectrum is not very sensitive to these parameters).

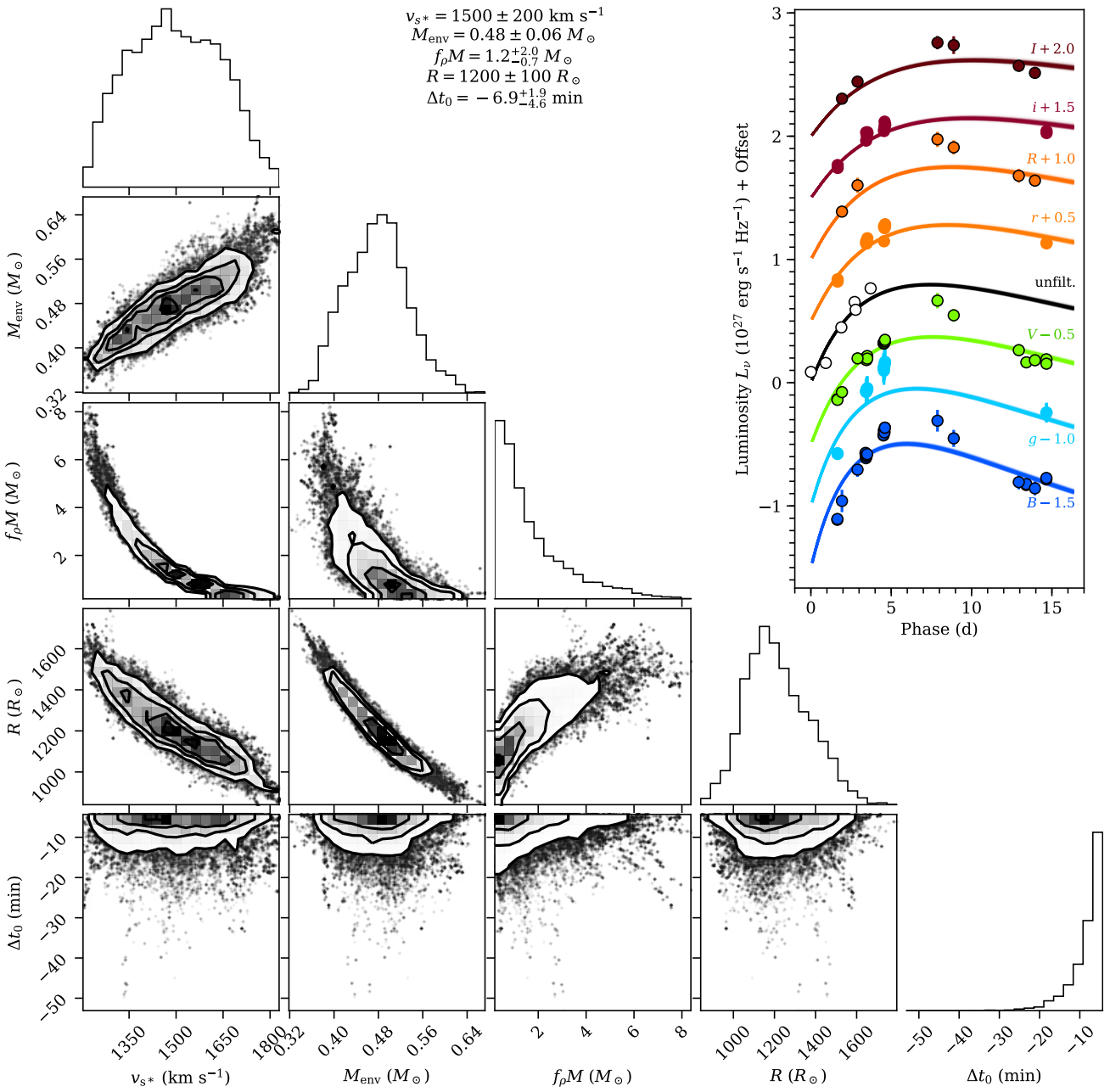

Figure 4. Posterior probability distributions of and correlations between the shock speed, v_{s*}; the mass of the progenitor envelope, M_{env}; the product of a numerical factor that describes the inner envelope structure, f_ρ, and the total ejected mass, M; the progenitor radius, R; and the time between explosion and discovery, Δt_0. The 1σ credible intervals centered around the median are given at the top. The top-right panel shows 100 fits randomly drawn from our MCMC routine compared to the data. (The fits appear to be single lines because the spread in the parameters is small.) We do not consider the shock cooling models to be a good fit to the light curve peak, leaving circumstellar interaction as the most probable power source.

Although the line positions match the observed spectrum quite well, a quadratic warping function is necessary to suppress the blue end of the model to match the observations. This function has no physical basis, but deviations from a perfect blackbody continuum with no electron scattering are conceivable. Another possibility is that our spectrograph has lost some of the blue light from the supernova in a way we have not sufficiently accounted for.

4.4. *Nebular Spectrum*

A nebular spectrum, taken after the ejecta are mostly transparent to optical light, provides an alternate method of estimating the progenitor mass. Following Jerkstrand et al. (2014), we estimate the mass of oxygen present in the progenitor by measuring the com-

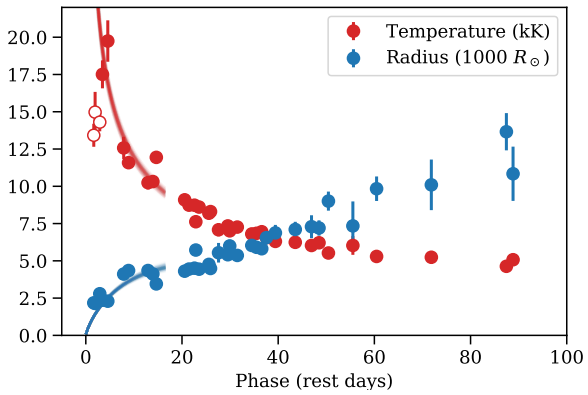

Figure 5. Best-fit blackbody temperature (red points) and radius (blue points) of SN 2016bkv during the photospheric phase, compared to the temperature (red lines) and radius (blue lines) from the best-fit Sapir & Waxman (2017) models in Section 4.2. The open red points are likely underestimates of the temperature from when the SED peaks blueward of our observations.

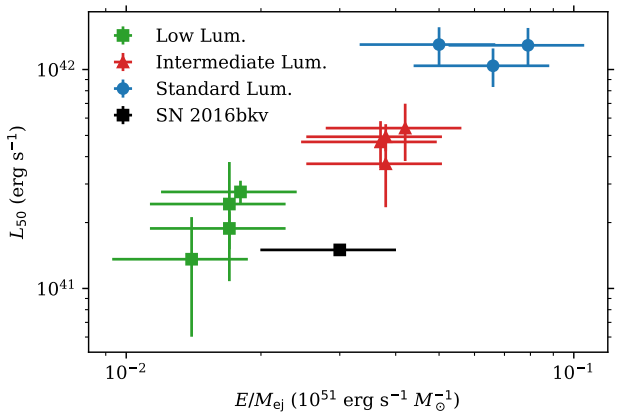

Figure 6. Correlation between plateau luminosity and photospheric velocity for the sample of Pumo et al. (2017, compare their Figure 5). SN 2016bkv fits relatively well into their LL SN II category, although it has a slightly higher ratio of energy to ejecta mass. Keep in mind that the $E/M_{\rm ej}$ measurement comes from the shock cooling models, which we do not believe are a good fit.

bined luminosity of the forbidden oxygen lines at 630.0 and 636.4 nm. The ratio of this mass to the nickel mass produced in the explosion (as measured through the bolometric luminosity in the nebular phase; see Section 4.1) is sensitive to the progenitor mass.

The oxygen lines in question are not detected in our spectrum at 257 days, perhaps because the low ejecta velocity causes slower evolution than in other SNe II. We find the oxygen luminosity 435 days after explosion to be consistent with the 15 $M_\odot$ progenitor model of Jerkstrand et al. (2014). Figure 9 shows this measurement in comparison with other SNe II from Valenti et al. (2016, their Figure 24). However, as Jerkstrand et al. (2014, their Footnote 5) note, these models were derived using parameters that may not be suitable for LL SNe II. Therefore, this should only be treated as an approximate result.

5. CONCLUSIONS

Two lines of evidence point to strong but short-lived circumstellar interaction in SN 2016bkv. First, flash spectroscopy during the first five days reveals the presence of material around the progenitor star. A few days later, the light curve shows a strong peak as the ejecta interact with this material, adding luminosity on top of the plateau powered by recombination of the hydrogen envelope. This peak cannot be fit with shock cooling models alone. Even with this strong early peak at $M_V = -16.1$, SN 2016bkv is the lowest-luminosity supernova to show flash ionization lines, suggesting that late-stage mass loss is common among RSGs.

SN 2016bkv is also exceptional in its short fall from plateau, indicating a large nickel production (0.015 $M_\odot$) compared to other LL SNe II. Despite this, our analysis of the nebular spectrum suggests it had a fairly typical 15 $M_\odot$ RSG progenitor. This seems to support neither the high-mass-progenitor/fallback-SN scenario nor the low-mass-progenitor/electron-capture-SN scenario. Rather, it is perfectly consistent with the 8.5 to 16.5 $M_\odot$ RSG progenitors for SNe II observed with *HST*.

This and other lines of evidence suggest that analyses of SNe II should be careful to distinguish between the properties of the progenitor star itself and the properties of its circumstellar environment. Peak luminosity, for example, is strongly affected by circumstellar interaction, whereas luminosity after settling on the plateau may be related to the progenitor star. Future data sets like the one presented here, with early and long-term coverage of young supernovae, will allow us to constrain progenitor properties and mass-loss history separately, by comparing to numerical light-curve and spetral models.

G.H., C.M., and D.A.H. are supported by the National Science Foundation under grant No. 1313484. Support for I.A. was provided by NASA through the Einstein Fellowship Program.

Facilities: ADS, Beijing:0.8m, Beijing:2.16m (BFOSC, OMR), Keck:I (LRIS), LCOGT (FLOYDS, Sinistro, Spectral), NED, Shane (Kast)

Software: Astropy (Astropy Collaboration 2013), `emcee` (Foreman-Mackey et al. 2013), `lcogtsnpipe` (Valenti et al. 2016), PyRAF (Science Software Branch at

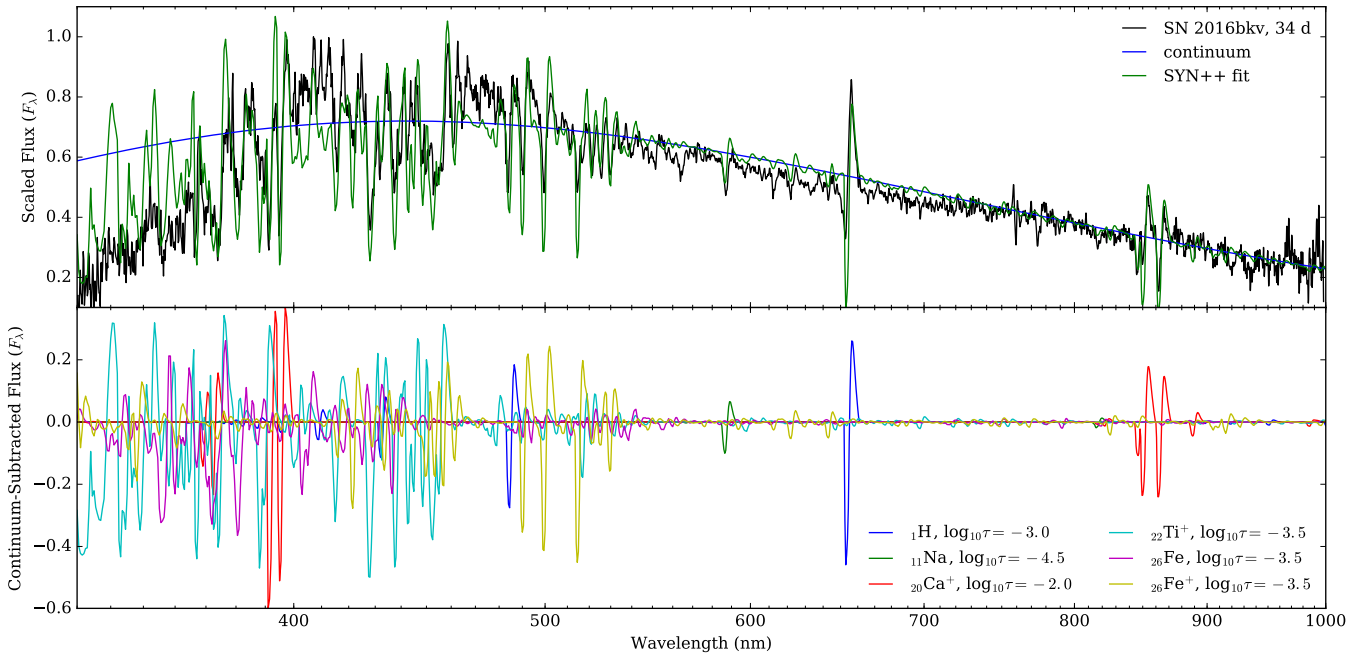

Figure 7. SYN++ model for the spectrum of SN 2016bkv 34.7 days after maximum light. The top panel shows the observed spectrum, the assumed continuum (a 7500 K blackbody warped by a quadratic polynomial; see Section 4.3), and the total synthetic spectrum (also warped). The bottom panel shows the contributions to the synthetic spectrum of each of the six ions we consider. (The SYN++ input file used to create this figure is available.)

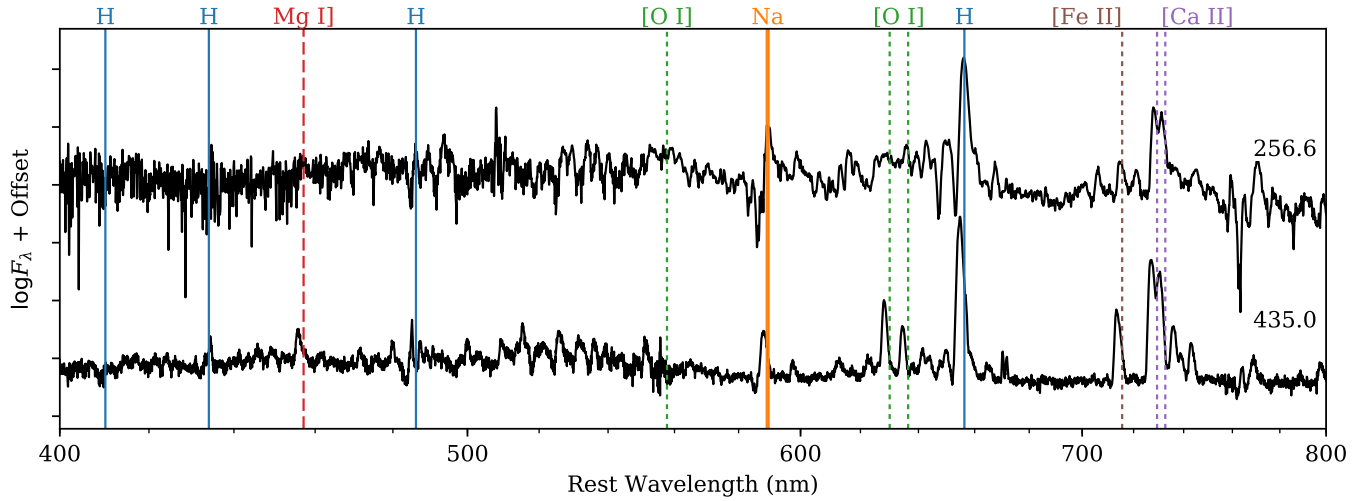

Figure 8. Nebular spectra of SN 2016bkv taken at 257 and 435 days after estimated explosion. Our analysis focuses on the forbidden O I lines (green dotted lines).

STScI 2012), PyZOGY (Guevel & Hosseinzadeh 2017), SExtractor (Bertin & Arnouts 1996), SNOoPY (Cappellaro 2016), SYN++ (Thomas et al. 2011)

REFERENCES

Adelman-McCarthy, J. K., Allam, S. S., Allende Prieto, C., et al. 2007, ApJS, 175, 297

Aihara, H., Allende Prieto, C., An, D., et al. 2011, ApJS, 193, 29

Astropy Collaboration, Robitaille, T. P., Tollerud, E. J., et al. 2013, A&A, 558, A33

Barbon, R., Buondi, V., Cappellaro, E., & Turatto, M. 2008, yCat, 1, 2024

Barbon, R., Ciatti, F., & Rosino, L. 1979, A&A, 72, 287

Benetti, S., Patat, F., Turatto, M., et al. 1994, A&A, 285, L13

Bertin, E., & Arnouts, S. 1996, A&AS, 117, 393

Brown, T. M., Baliber, N., Bianco, F. B., et al. 2013, PASP, 125, 1031

Cappellaro, E. 2016, SNOoPY: a package for supernova photometry, v.0.6, http://sngroup.oapd.inaf.it/snoopy.html

Chugai, N. N. 1991, MNRAS, 250, 513

Chugai, N. N., & Utrobin, V. P. 2000, A&A, 354, 557

Fan, Z., Wang, H., Jiang, X., et al. 2016, PASP, 128, 115005

Ferrarese, L., Mould, J. R., Kennicutt, R. C., et al. 1999, ApJ, 529, 745

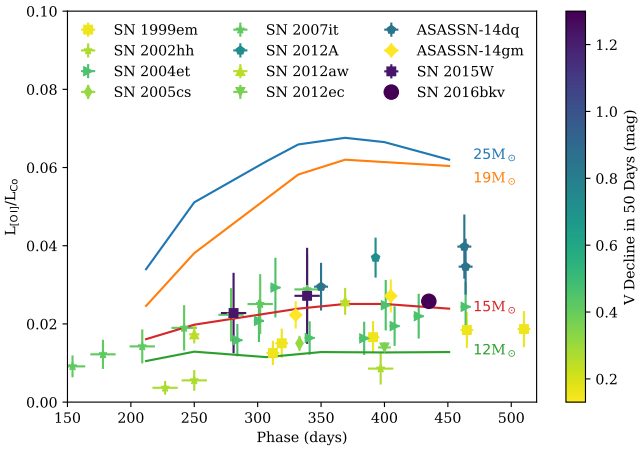

Figure 9. Oxygen luminosity in the nebular spectra of SNe II (Valenti et al. 2016) compared to models (Jerkstrand et al. 2014). SN 2016bkv is consistent with having a 15 $M_{\odot}$ progenitor.

Foreman-Mackey, D., Hogg, D. W., Lang, D., & Goodman, J. 2013, PASP, 125, 306

Gal-Yam, A., Arcavi, I., Ofek, E. O., et al. 2014, Natur, 509, 471

Garnavich, P. M., & Ann, H. B. 1994, AJ, 108, 1002

Guevel, D., & Hosseinzadeh, G. 2017, PyZOGY, v.0.0.1, Zenodo, doi:10.5281/zenodo.1043973

Hamuy, M. 2003, ApJ, 582, 905

Hamuy, M., & Pinto, P. A. 2002, ApJ, 566, L63

Hodge, P. W., & Kennicutt, Jr., R. C. 1983, AJ, 88, 296

Hosseinzadeh, G., Howell, D. A., Arcavi, I., McCully, C., & Valenti, S. 2016, TNSCR, 239, 1

Huang, F., Li, J.-Z., Wang, X.-F., et al. 2012, RAA, 12, 1585

Itagaki, K. 2016, TNSTR, 234, 1

Jerkstrand, A., Smartt, S. J., Fraser, M., et al. 2014, MNRAS, 439, 3694

Jones, M. I., Hamuy, M., Lira, P., et al. 2009, ApJ, 696, 1176

Khazov, D., Yaron, O., Gal-Yam, A., et al. 2016, ApJ, 818, 3

Landolt, A. U. 1992, AJ, 104, 340

Leonard, D. C., Filippenko, A. V., Barth, A. J., & Matheson, T. 2000, ApJ, 536, 239

Li, W., Van Dyk, S. D., Filippenko, A. V., et al. 2006, ApJ, 641, 1060

Matheson, T., Filippenko, A. V., Barth, A. J., et al. 2000, AJ, 120, 1487

Matzner, C. D., & McKee, C. F. 1999, ApJ, 510, 379

Maund, J. R., Smartt, S. J., & Danziger, I. J. 2005, MNRAS, 364, L33

Milisavljevic, D., Chilingarian, I., Berlind, P., et al. 2016, ATel, 8861, 1

Miller, J. S., & Stone, R. P. S. 1994, The Kast Double Spectograph, Lick Observatory Technical Reports No. 66 (Santa Cruz: Lick Observatory)

Morozova, V., Piro, A. L., & Valenti, S. 2017a, arXiv:1709.04928

—. 2017b, ApJ, 838, 28

Niemela, V. S., Ruiz, M. T., & Phillips, M. M. 1985, ApJ, 289, 52

Oke, J. B., Cohen, J. G., Carr, M., et al. 1995, PASP, 107, 375

Pastorello, A., Zampieri, L., Turatto, M., et al. 2004, MNRAS, 347, 74

Patat, F., Barbon, R., Cappellaro, E., & Turatto, M. 1994, A&A, 282, 731

Pejcha, O., & Prieto, J. L. 2015, ApJ, 806, 225

Pierce, M. J. 1994, ApJ, 430, 53

Pumo, M. L., Zampieri, L., Spiro, S., et al. 2017, MNRAS, 464, 3013

Quimby, R. M., Wheeler, J. C., Höflich, P., et al. 2007, ApJ, 666, 1093

Rockosi, C., Stover, R., Kibrick, R., et al. 2010, SPIE, 7735E, 0R

Ross, T. W., Channa, S., Molloy, J. D., Zheng, W., & Filippenko, A. V. 2016, ATel, 8875, 1

Sapir, N., & Waxman, E. 2017, ApJ, 838, 130

Schlegel, E. M. 1990, MNRAS, 244, 269

—. 2001, ApJ, 556, L25

Science Software Branch at STScI. 2012, PyRAF: Python alternative for IRAF, ASCL, http://ascl.net/1207.011

Shapley, H. 1939, PNAS, 25, 569

Shivvers, I., Groh, J. H., Mauerhan, J. C., et al. 2015, ApJ, 806, 213

Smartt, S. J. 2009, ARA&A, 47, 63

Smartt, S. J., Gilmore, G. F., Trentham, N., Tout, C. A., & Frayn, C. M. 2001, ApJ, 556, L29

Smith, N., Li, W., Silverman, J. M., Ganeshalingam, M., & Filippenko, A. V. 2011, MNRAS, 415, 773

Spiro, S., Pastorello, A., Pumo, M. L., et al. 2014, MNRAS, 439, 2873

Strauss, M. A., Huchra, J. P., Davis, M., et al. 1992, ApJS, 83, 29

Thomas, R. C., Nugent, P. E., & Meza, J. C. 2011, PASP, 123, 237

Turatto, M., Mazzali, P. A., Young, T. R., et al. 1998, ApJ, 498, L129

Valenti, S., Howell, D. A., Stritzinger, M. D., et al. 2016, MNRAS, 459, 3939

Yaron, O., & Gal-Yam, A. 2012, PASP, 124, 668

Yaron, O., Perley, D. A., Gal-Yam, A., et al. 2017, NatPh, 13, 510

Zackay, B., Ofek, E. O., & Gal-Yam, A. 2016, ApJ, 830, 27

Zampieri, L., Shapiro, S. L., & Colpi, M. 1998, ApJ, 502, L149